Role of Zn and Polyaniline in Magnetic Nanocomposites and Enhanced Arsenic Adsorption Capacity in Wastewater

Tran Minh Thi (tranminhthi5@duytan.edu.com)
Duy Tan University https://orcid.org/0000-0003-3146-7212
Nguyen Mau Lam
Hanoi Pedagogical University No 2, Vinh Phuc
Do Khanh Tung
Institute of Materials Science, Vietnam Academy of Science and Technology, Vietnam
Nguyen Manh Nghia
Hanoi National University of Education
Duong Quoc Van
Hanoi National University of Education
Vu Quoc Manh
Faculty of Pharmacy, Thanh Do University
Nguyen Thi Bich Viet
Faculty of Chemistry, Hanoi National University of Education
Duong Khanh Linh
Faculty of Chemistry, Hanoi National University of Education
Vu Quoc Trung
Faculty of Chemistry, Hanoi National University of Education
Nguyen Thuy Chinh
Institute for Tropical Technology, Vietnam Academy of Science and Technology
Thai Hoang
Institute for Tropical Technology, Vietnam Academy of Science and Technology

Research Article

Keywords: adsorption ability, magnetization, infrared spectra, polyaniline/Fe0.90Zn0.10Fe2O4 nanocomposites

Posted Date: June 30th, 2022

DOI: https://doi.org/10.21203/rs.3.rs-1176740/v2

Abstract

The nanoparticles of Polyaniline/$Fe_{0.90}Zn_{0.10}Fe_2O_4$ (PANI/$Fe_{0.90}Zn_{0.10}Fe_2O_4$) were synthesized by a co-precipitation method and an in-situ polymerization method. XRD patterns showed that the $Fe_{0.90}Zn_{0.10}Fe_2O_4$ grain size about 11.8 nm, while TEM image showed grain size from 10 to 18 nm. The results of FT-IR spectra and DTA analyses showed that PANI participated in nanocomposite samples. The grain size of PANI/$Fe_{0.90}Zn_{0.10}Fe_2O_4$ samples measured by SEM was about 35–50 nm. The magnetization measurements showed that the saturation magnetic moment of PANI/$Fe_{0.90}Zn_{0.10}Fe_2O_4$ samples at 300 K decreased from 71.5 to 43 emu/g when PANI/$Fe_{0.90}Zn_{0.10}Fe_2O_4$ mass ratio increased from 0–40%. The arsenic adsorption capacity of nanocomposite samples with different PANI concentration was investigated in solutions of pH 1 to pH 14. The q_{max} maximum arsenic adsorption capacities were calculated by the Langmuir isotherm equation at pH 7 and 300 K. The evaluated results show that with mass ratio of 0.9%, the sample S_1 with q_{max} = 43.48 mg/g is higher than that Fe_3O_4 nanoparticles. In addition, the substitution of Fe^{2+} ions by Zn^{2+} ions in $Fe_{0.90}Zn_{0.10}Fe_2O_4$ and PANI coating were improving more magnetic and chemical stable of samples over time. Other hand, these materials could be reused after desorption in solution at pH 14.

Introduction

Nanocomposite materials of ferrite and polymer attract attention of the scientists due to their wide applications in engineering (Chao Lian et al 2017; Cîrcu M et al 2018), in biomedical applications (Amir Aziz et al 2020; Fizesan I et al 2021; Mohamed Alae Ait Kerroum et al 2020), especially in water treatment (Babu CM et al 2018; Khodabakhshi A et al 2011; Ruijiang Liu et al 2013; Huiping Zeng et al 2020) or environmental pollution monitoring (Adeleke J. T et al 2018; Shah M. T et al 2018; Lixin Yu et al 2018). The important reason for this problem is that the magnetic nanocomposite materials are easy to recover and reuse, whereas the removals of Cd, Cr, As using nonmagnetic metal oxide hetero-structures, and meso-porous (Lei Chen et al 2014; Xiaolong Li et al 2012; Zapotoczny B et al 2012; Lia Méndez-Rodríguez et al 2013; Kuen-Song Lin et al 2013) are very difficult in recovery and thus leaving residuals in the environment. In this circumstance, magnetic nanoporous materials are considered as potential candidates for heavy metal removal because it's simple and efficient to recover them from the solution by external magnetic field.

Due to the rapid oxidation of Fe_3O_4 into γ-Fe_2O_3 in air as well as its magnetization decreased, large numbers of studies have focused on improving the saturation magnetization and chemical stability of the magnetic nanomaterials in order to effective heavy metal ion adsorption (Ruijiang Liu et al 2013; Park J. W et al 2013; Zaki H. M et al 2013; Larumbe S et al 2012; Deepshikha Rathore et al 2013; Genç F et al 2015). Two research directions are being considered: *(i)* partial replacement of divalent metal ions for Fe^{2+} ions, and *(ii)* coating of magnetic nanoparticles by polymers.

In the direction of Fe^{2+} ion replacement research in Fe_3O_4, in which the unit cell of Fe_3O_4 consists of two kinds of interstitial sites $\left[Fe^{3+}\right]_A\left[Fe^{3+}Fe^{2+}\right]_B$ denoted as tetrahedral A-site (Fe^{3+}) and octahedral B-site (Fe^{2+}:Fe^{3+}=1:1) (Park J. W eta al 2013; Larumbe S et al 2012), the divalent metal ions like Mn^{2+}, Cu^{2+} and Ni^{2+} are usually substituted into B-site to form inverse spinel ferrites such as $Fe_{1-x}M_xFe_2O_4$ (with M = Mn^{2+}, Co^{2+}, Cu^{2+}, Ni^{2+}, Mg^{2+}) (Aparna M. L et al 2018; Sudheesh V. D et al 2018; Shah M. T et al 2018; Tran Minh Thi et al 2015). However, the substitutions of Zn^{2+} ions for Fe^{2+} ions in $Fe_{1-x}Zn_xFe_2O_4$ (x = 0; 0.2; 0.4; 0.5) thin films or nanopowders with pretty large magnetization were confirmed by the partial substitutions of Zn^{2+} ions into A-sites (Park J. W et al 2013; Tran Minh Thi et al 2021). The partial substitution of Zn^{2+} ions for Fe^{2+} ions makes more stable in terms chemical and magnetic properties of nanomaterials (Tran Minh Thi et al 2021) and improves applicability.

Recently, the magnetic nanoparticles are studied to treat heavy metals, weak-acid oxyanion contaminants (Uwamariya V et al 2015; Kiril D et al 2017; Huda Faker et al 2015; Huiping Zeng et al 2020) or dyes in wastewater environment (Adeleke J. T et al 2018). However, the coating of magnetic nanoparticles by polymers are also studied to protect the chemical physical properties of magnetic nanoparticles simultaneously to ensuring the recovery and reuse of adsorbent materials (Sadia Ameen et al 2010; Minh Thi Tran et al 2016). In recent, the substitution of Mn^{2+}, $Cu^{2)}$, Zn^{2+} ions for Fe^{2+} ion and the coating of magnetic nanoparticles by polyaniline (PANI), poly(1-naphthylamine), polyvinyl pyrrolidone (Gabal M. A et al 2018; Tran Minh Thi et al 2021; Minh Thi Tran et al 2016) have been studied to stabilize the physicochemical properties and enhance their applicability, but the obtained results are very different and have not yet paid attention to the physicochemical stability and the reusability of the materials.

In this work, the article presents the following issues:

- Microstructure research of nanocomposites with different PANI/$Fe_{0.90}Zn_{0.10}Fe_2O_4$ mass ratios, that synthesized by the combination of co-precipitation method and in-situ polymerization method.

- Research of role of the Zn^{2+} ion substitution for Fe^{2+} ions and PANI in order to physicochemical characteristic stability of PANI/$Fe_{0.90}Zn_{0.10}Fe_2O_4$ nanocomposites.

- The arsenic adsorption ability in aqueous at different pH values, maximum arsenic adsorption capacity as well as the desorption/re-adsorption capacities of the magnetic composite nanomaterials are also discussed.

Experiment

Chemical and apparatus

All chemicals are at analytical grade: $FeCl_3.6H_2O$, Na_2SO_3, 25% NH_3, $Zn(CH_3COO)_2.2H_2O$, NaOH, HCl, acetone 99%, isopropanol (IPA), $(NH_4)_2S_2O_{8,}$ As(III) solutions in which the As(III) content of 106 ppb, 10

times higher than allowed levels regulated by the World Health Organization (WHO) were prepared from As_2O_3. Labconco Freeze Concentrator (USA) was used for material drying in vacuum. The structure and morphology of the samples were investigated by XRD patterns (D5005, Bruker), TEM (JEOL5410), SEM (S4800), IR Prestige − 21 and thermal gravimetric analysis (TGA) by DTG- 60H. Meanwhile the magnetization was measured by vibrating sample magnetometer (VSM 8600 S) and the mesoporous structure of samples was observed by TriStar 3000 V6.07A with TriStar 3000 V6.08 software. The Flame-Atomic Absorption Spectrophotometer (F-AAS 6300 Shimadzu) was used to determine the arsenic content in the solutions before and after using adsorbent magnetic nanomaterials.

Synthesis of $Fe_{0.90}Zn_{0.10}Fe_2O_4$ by co-precipitation method

A detailed synthesis procedure was described in our previous paper (Minh Thi Tran et al 2016; Tran Minh Thi et al 2021). The chemical reactions occur during the synthesized process of Fe_3O_4:

$2FeCl_3 + Na_2CO_3 + H_2O \rightarrow 2FeCl_2 + Na_2SO_4 + 2HCl$ (1)

$2FeCl_3 + FeCl_2 + 8NH_3 + 4H_2O \rightarrow Fe_3O_4\downarrow + 8NH_4Cl$ (2)

To get $Fe_{2.9}Zn_{0.10}O_4$ (signed $Fe_{0.90}Zn_{0.10}Fe_2O_4$) nanoparticles, the $FeCl_3{\cdot}6H_2O$, $Zn(CH_3COO)_2{\cdot}4H_2O$ solutions containing $Fe^{3+}$and $Zn^{2+}$with nominal Zn atom content of 0.10 were mixed with a Na_2SO_3 solution. These mixed solutions were stirred until they turned to yellow in color. Then, the NH_3 solution was added dropwise until the pH was 10. The solution was kept stirring for 30 minutes until it turned to black. These magnetic grains were separated from the mixture solution using external magnets, and then filtered, washed with distilled water. Finally, these materials were desiccated at 50 ^{0}C for 48 hours and finely grinded to obtain $Fe_{0.90}Zn_{0.10}Fe_2O_4$ nanoparticles.

Synthesis of PANI/$Fe_{0.90}Zn_{0.10}Fe_2O_4$ nanocomposites by in-situ polymerization method

The synthesis of PANI/$Fe_{0.90}Zn_{0.10}Fe_2O_4$ nanocomposite by in-situ polymerization method, in which the aniline monomers adsorbed on the surface of inorganic particles then polymerize aniline by the catalyst $(NH_4)_2S_2O_8$ to polyaniline (PANI). From there, the inorganic particles were coated with PANI, precipitated and separated from the solution. This synthesis method was briefly described as follow:

- A calculated amount of $Fe_{0.90}Zn_{0.10}Fe_2O_4$ was added in 60 mL of distilled water, followed by 40 mL of IPA, aniline and well stirred for 60 minutes (mixture A).

- A amount of $(NH_4)_2S_2O_8$ solution, with the monomer/oxidizing agent molar ratio of 1:1.5 was added dropwise into mixture A to obtain a black blue mixture (mixture B) which was allowed to stir for 2 hours with an exothermal reaction.

- Filter the mixture using external magnet, then the obtained solid was dried by Labconco Freeze concentrator for 5 hours at 1 mPa and temperature of 40^{o}C. The nanocomposites with different mass ratios of PANI/$Fe_{0.90}Zn_{0.10}Fe_2O_4$ were synthesized by in situ polymerization method of aniline on the surface of $Fe_{0.90}Zn_{0.10}Fe_2O_4$ particles and coded by S_0, S_1, S_2 and S_3 as represented in Table 1.

Table 1
Aniline, PANI component in S_0, S_1, S_2, S_3 samples.

Sample	S_0	S_1	S_2	S_3
$Fe_{0.90}Zn_{0.10}Fe_2O_4$, (in g)	20	20	20	20
Aniline (ml)	0	1,8	5,1	7,8
Mass ratio (PANI/$Fe_{0.90}Zn_{0.10}Fe_2O_4$)	0%	9%	26%	40%

Thermal properties and temperature-induced mass changes were investigated for PANI and representative S_2 sample by DTA measurement. Then the mass ratios of PANI/$Fe_{0.90}Zn_{0.10}Fe_2O_4$ in the samples (in Table 1) are calculated by values of saturation magnetization measurements using VSM below.

The evaluation of arsenic adsorption

The adsorption kinetic of nanocomposites was studied by the nitrogen adsorption-desorption isotherms of S_0, S_1, S_2 and S_3 samples at 77 using BET method. The evaluation of arsenic adsorption capacity of the samples was performed at room temperature. The experiment was conducted by adding 0.01 g of samples (S_0, S_1, S_2 and S_3) into As(III) solutions of initial content of 106 ppb. Each mixture was then allowed to stir in 50–60 minutes for a complete adsorption. The arsenic contents before and after adsorption were analyzed by Flame-Atomic Absorption Spectrophotometer F-AAS.

Results And Discussion

Structure, morphology of samples

In Fig. 1, the diffraction peaks of (220), (311), (400), (442), (511), (440) of the $Fe_{0.90}Zn_{0.10}Fe_2O_4$ (S_0) sample were completely fitted with the standard diffraction pattern of Fe_3O_4 as in previous publication (Tran Minh Thi et al 2021), and demonstrated the centered face cubic structure. Unlike the replacement of Cu^{2+}, Mn^{2+}, Ni^{2+} transition metal ions for Fe^{2+} into octahedral B-site (Zaki H. M et al 2013; Larumbe S et al 2012; Deepshikha Rathore et al 2013; Aparna M. L et al 2018), preferably the replacement of Zn^{2+} ions for Fe^{3+} at tetrahedron A-site occurs, simultaneously Fe^{2+} amount at the octahedral B-site gives electrons to become Fe^{3+} in order to balance the charge of cell network (Park J. W et al 2013; Deepshikha Rathore et al 2013). Since the ionic radius of the Fe^{3+} ion is 0.64 Å and the ionic radius of the Zn^{2+} ion is 0.74 Å, the substitution of Zn with content x = 0.10 caused a slight increasing of the lattice constant (a =

8.386 A^0) in comparison with Fe_3O_4 (a = 8.3760 A^0) (Tran Minh Thi et al 2015; Tran Minh Thi et al 2021), which was determined by the relation: $a = d_{hkl}\sqrt{h^2 + k^2 + l^2}$; where d_{hkl} is the distance of the lattice planes of $Fe_{0.90}Zn_{0.10}Fe_2O_4$.

Similarly, the XRD patterns of S_1, S_2 and S_3 samples showed the same diffraction peaks as that of Fe_3O_4 sample, which proved that the Zn^{2+} doping as well as the addition of polymer did not affect the crystal structure of materials. From diffraction conditions, $2d\sin\theta = n\lambda$, the lattice constants of the nanoparticles in the S_0, S_1, S_2 and S_3 samples were the same with a = 8.376 A^0

Because PANI polymer is an amorphous material and does not affect the crystal structure of $Fe_{0.90}Zn_{0.10}Fe_2O_4$ nanoparticle, thus the calculated crystal particle size from XRD pattern is also the crystal particle size for S_1, S_2 and S_3 samples about 11.8 nm, that were calculated by the formula $D = 0.9\lambda/\beta\cos\theta$ (λ = 1.5416 A^0; β: full width at haft maximum of diffraction line). In Fig. 2a, the TEM image of S_0 sample shows the grain sizes about of 10–18 nm, however, the SEM image in Fig. 2b show the agglomeration in S_1 sample with grain size about of 40–50 nm due to the presence of PANI in the sample. Meanwhile, in SEM images in Fig. 2c and Fig. 2d, the grain sizes in S_2, S_3 samples were about 35–50 nm and 40–50 nm.

FT-IR spectra analyses

FT-IR spectrum in Fig. 3a shows strong absorbed peaks of PANI in the region from 1149.6 to 1573.5 cm^{-1} with the highest intensity at 1149.6 cm^{-1} peak. The peaks of 1149.6 cm^{-1}, 1303.9 cm^{-1} were attributed to the absorption of bending vibrating of C-H, stretching vibrating of C-N^+ groups. The peaks of 1400.3 cm^{-1}, 1492.6 cm^{-1} were attributed to the absorption of stretching vibrating of C-N groups and 1573.5 cm^{-1} peak of C = C group in PANI (Bogdan Butoi et al 2017). Figure 3b shows the strong adsorbed peak of S_0 at 571 cm^{-1} and two small peaks of 1400.3 cm^{-1}, 1623 cm^{-1}. Meanwhile, Fig. 3c shows the vibrating peak appearances of 1573.5 cm^{-1}; 1492.6 cm^{-1}, 1303.9 cm^{-1} and 1134 cm^{-1} and the small shift of 571 cm^{-1} and 1134 cm^{-1} peaks were suggested that PANI is present in the component of S_2. The vibrational modes observed in the FT-IR spectra of PANI, S_0, S_2 samples were presented in Table 2

Table 2
Vibrational modes observed in the FT-IR spectra of PANI, S_0, S_2 samples

PANI		S_0	S_2
Wavenumber (cm^{-1})	Vibrational modes	Wavenumber (cm^{-1})	Wavenumber (cm^{-1})
3124.5	vibrating of OH	3124.5–3370	3190.1; 3375.4
1573.5; 1492.6	vibrating of C = C group	1623	1573.5; 1492.6
1400.3; 1303.9	vibrating of C-H, $C\text{-}H^+$ group	1400.3	14003; 1303.9
1149.6	bending vibrating of C-H		1134
821.7; 594.1		571	571

TGA and DTG analyses

Thermal properties of PANI and composite samples were investigated by thermal gravimetric analysis for PANI and representative S_2 sample

TGA curve in Fig. 4a showed that at temperature range below 80 ^{0}C, the mass reduction of PANI was due to the evaporation of water, corresponding to 13% with a sharp endothermic peak at 45 ^{0}C in the DTG curve. From 80–210 ^{0}C, the sample mass stays almost unchanged. However, from 210–320 ^{0}C, the reduction of sample mass in TGA curve happened due to the decomposition of PANI to form monomers, oligomers, dimers and trimers corresponding to a sharp endothermic peak at 292 ^{0}C in the DTG curve. At temperature higher than 320 ^{0}C, the weight loss caused by the thermal decomposition of the oligomers, dimers, trimers. This led to a complete decomposition of PANI at above 600 ^{0}C.

TGA curve of typical S_2 sample in Fig. 4b also showed that at temperature range below 80 ^{0}C, the 8.6% reduction of sample mass due to water evaporation corresponding to a sharp endothermic peak at 45.2 ^{0}C in the DTG curve. However, from 100–300 ^{0}C in the TGA curve, the 3.3% reduction of sample mass may be happened due to the decomposition of the residual monomers and oligomers in the sample. From 300–600 ^{0}C, the thermal decomposition of the oligomers, dimers, trimers caused a small and broad endothermic peak at 395 ^{0}C in the DTG curve. Thus, the sample mass remained only 28–29% that is attributed to remain component of $Fe_{0.90}Zn_{0.10}Fe_2O_4$ at 600 ^{o}C. It can be seen from above results that PANI is quite stable in the temperature range below 210 ^{o}C, thus the S_1, S_2 and S_3 samples have been successfully synthesized and the presence of PANI in these samples has improved the thermal stability of PANI-coated $Fe_{0.90}Zn_{0.10}Fe_2O_4$ nanoparticles.

Magnetization and chemical stability

The magnetization curves of samples show a decrease in saturation magnetization (Ms) with increasing PANI content (Fig. 5), where Ms of S_0 is the largest (71.5 emu/g). These issues are explained as follows:

The inverse-spin Fe_3O_4 is denoted as $[Fe^{3+}]_A[Fe^{3+}Fe^{2+}]_B$ (Park J. W et al 2013; Tran Minh Thi et al 2015; Tran Minh Thi et al 2021) with the Fe^{3+} ions in the tetrahedral (A)-sites and Fe^{2+} ions in octahedral (B)-sites (Fe^{2+}:Fe^{3+} = 1:1). Due to the replacement of Zn^{2+} ions for Fe^{3+} at tetrahedral A-site occurs, simultaneously Fe^{2+} amount at the octahedral B-site gives electrons to become Fe^{3+} in order to balance the charge of cell network (Park J. W et al 2013; Deepshikha Rathore et al 2013). These substitution and transformation caused a change in ion distribution of the network subdivisions to $\left[Zn_x^{2+}Fe_{1-x}^{3+}\right]_A\left[Fe^{3+}Fe_x^{3+}Fe_{1-x}^{2+}\right]_B$ (x = 0.05 ÷ 0.25) were explained clearly in recent work (Tran Minh Thi et al 2021). On the other hand, due to the magnetic moments of the Fe^{2+}, Fe^{3+} and Zn^{2+} ions are 5 μB, 4 μB and zero, respectively (Jun Liu et al 2012; Tran Minh Thi et al 2021), thus, at low temperature without an external field, the magnetic moment of ions at tetrahedral (A)-sites $\left[Zn_x^{2+}Fe_{1-x}^{3+}\right]_A$ is 4(1-x) μB, and the magnetic moment of ions at octahedral (B)-sites $\left[Fe^{3+}Fe_x^{3+}Fe_{1-x}^{2+}\right]_B$ is [4 + 4x + 5(1−x)] μB = (9−x) μB, with $0 \leqslant x < 1$. These magnetic moments are antiparallel and not offset with each other. In another aspect, at high temperature in external fields, the superexchange interactions between the magnetic moments of the (A) and (B) supernetworks depend on the doped content x, distance between magnetic ions and their angles with O^{2-} ions (Park J. W et al 2013; Tran Minh Thi et al 2021). Therefore, the saturation magnetization of $Fe_{0.90}Zn_{0.10}Fe_2O_4$ (here x = 0.10) is higher than Fe_3O_4 in external fields (Tran Minh Thi et al 2015; Tran Minh Thi et al 2021). In the air environment, Fe_3O_4 is easy to be oxidized to give γ-Fe_2O_3. Thus, the saturation magnetization of new synthesized Fe_3O_4 samples decreased strongly after 2 months of synthesis (Tran Minh Thi et al 2015) that related the oxidation of Fe_3O_4 into γ-Fe_2O_3 due to oxygen in air according to the equation:

$$4Fe_3O_4 + O_2 \rightarrow 6Fe_2O_3 \quad (3)$$

According to (3), the partial substitution of Zn^{2+} ions for Fe^{2+} will reduce sample oxidation to Fe_2O_3. Thus, the Zn^{2+} substitution for Fe^{2+} ions and the polymer coating outside nanoparticles are the optimal methods to stabilize chemical properties and magnetization of $Fe_{0.90}Zn_{0.10}Fe_2O_4$ material.

On the other hand, the Ms measurements of S_1, S_2 and S_3 samples show that the saturation magnetizations of S_1, S_2 and S_3 samples decreased from 65 emu/g to 43 emu/g due to the increase of non-magnetic PANI content. In addition, S_1, S_2, S_3 samples have similar magnetic material composition as S_0 sample, so after synthesization the real mass ratios of PANI/$Fe_{0.90}Zn_{0.10}Fe_2O_4$ in S_0, S_1, S_2 and S_3 samples are calculated 0%, 9%, 26% and 40% as shown in Table 1. The calculated result of PANI/$Fe_{0.90}Zn_{0.10}Fe_2O_4$ mass ratio in sample S_2 is quite consistent with the results of the survey on the loss of mass of typical S_2 sample by DTA measurement in Fig. 4. Furthermore, the specific mass of PANI

is less than that of the ferromagnetic particles, thus, the particle sizes in samples S_1, S_2 and S_3 are larger than that of sample S_0 due to PANI coating (Fig. 2.b,c,d)

Table 3
Lattice constant, grain size and Ms

	Lattice constant (A^0)	$D_{x\text{-}ray}$ (nm)	D_{TEM} (nm)	D_{SEM} (nm)	Ms (emu/g)
S_0	8.385	11.81	10–18		71.5
S_1	8.385	11.80		40–50	65
S_2	8.386	11.80		35–50	53
S_3	8.386	11.81		40–50	43

However, due to the PANI coating, the magnetization and chemical properties of nanocomposite materials is more stable over time.

Adsorption kinetic, porous properties and arsenic adsorption ability

Adsorption kinetic and porous properties

The adsorption kinetic of S_0, S_1, S_2 and S_3 nanocomposites can be explained (Tran Minh Thi et al 2015; Minh Thi Tran et al 2016) by the relation of adsorption ability based on the inelastic exchange interaction between specific surface area of nanoparticles and adsorbed materials. The surface and structure of nanoparticle mesoporous were studied by the nitrogen adsorption-desorption isotherms of 0.54 g for S_0, S_1, S_2 and S_3 samples at 77 K (Tran Minh Thi et al 2015; Minh Thi Tran et al 2016).

Collision of N_2 gas molecules with nanoparticles is considered to be inelastic, so that the N_2 gas molecules remain in contact with the nanoparticles for a time before returning to the gas phase. This time delay is taken as responsible for the phenomenon of adsorption that demonstrated by equation: $P/V_a(P_0 - P) = (1/V_m)(P/P_0)$ (Paul A et al 1997). Here, V_a is the quantity of N_2 gas adsorbed at pressure P and V_m is the quantity of gas adsorbed when the entire surface is covered with a mono-molecular layer. The N_2 adsorption–desorption isotherm curves of S_0, S_1, S_2 and S_3 samples at 77 K were presented in Fig. 6. It can be clearly seen that the adsorption and desorption ability of S_1 sample is higher than that of S_0. By the BET (Brunauer, Emmett, and Taller) theory (Paul A et al 1997), the BET specific surface area at relative low pressure $P/P_0 = 0.294$ were calculated as shown in Table 4. Comparing the specific surface area of S_0 sample and S_1, S_2 and S_3 composite samples, it can be seen that although the particle sizes of S_1, S_2 and S_3 samples are larger than that of S_0 (TEM and SEM images in Fig. 2), but PANI coating increased

specific surface area of the material and achieved the highest specific surface area for S_1 sample with the appropriate PANI mass ratio.

Table 4
Porous properties and maximum arsenic adsorption ability

Sample (this study)	BET Desorption average pore diameter	BET specific surface area ± 0.02 (m^2/g) at P/Po = 0.294	Maximum adsorption capacity q_{max} (mg/g)	Sample type in reference of other works	q_{max} (mg/g)
S_0	118.839 Å	71.7685 m²/g	41.49	Fe_3O_4 nanoparticles (Khodabakhshi A et al 2011) Iron sludge (Huiping Zeng et al 2021)	23.8 mg/g 11.76mg/g 12.74mg/g
S_1	84.8842 Å	94.7092 m²/g	43.48	Chitosan-magnetic-graphene oxide (Sherlala, A. I. A et al 2019)	45 mg/g
S_2	88.1445 Å	90.9667 m²/g	40.06	Core–shell Fe3O4@SiO2 nanoparticles (Babu CM et al 2013)	16.58 mg/g
S_3	94.6178 Å	86.1750 m²/g	34.48	Magnetic graphene nanoplatelet with core-shell $Fe@Fe_2O_3$ nanoparticles (Jiahua Zhu et al 2012)	11.34mg/g

Arsenic adsorption ability

The effects of pH in environment and arsenic maximum adsorption capacity also were investigate at room temperature as follow.

Effects of pH on arsenic adsorption

To study the pH effect on the adsorption ability of the nanocomposite materials, the As(III) solutions with different pH in range of 1-14 were prepared. The As(III) adsorption results were presented in Fig. 7. After stirring the mixture of nano powder and arsenic solution for about 30-40 minutes, it can be seen from Fig. 7 that the remaining arsenic content was a function of the pH. For all nanocomposite samples, the arsenic adsorption capacity increased as the pH was increased from 1 to 7. Then, the adsorption capacity decreased as the pH was increased above 7. The highest adsorption capacities were obtained in the range about of pH 6-8.

In neutral media, the nanocomposites were stable with no iron and zinc ions detected in the solution and the un-charge in surface of As(III) (H_3AsO_3) at pH below 9.2 (Su H et al 2017), so at pH 7, the highest arsenic adsorption was occurred but not electrostatic interaction under this condition. Therefore, the As(III) adsorption was controlled by the surface complexation of composite nanoparticles at pH 7 media. Similar results were observed with other magnetic nanocomposites as reported earlier (Sherlala A. I. A et al 2019; Su H et al 2017).

In both strong acidic and basic solution, the adsorption capacity decreased. These issues are trying to explain by the characteristics of arsenic (III) at different pH media and the surface charge status of the nanocomposites (Sherlala A. I. A et al 2019) in strong acidic or base environments. At very low pH levels (pH from 1-2), the lest arsenic adsorption due to the decomposition of the $Fe_{0.90}Zn_{0.10}Fe_2O_4$ nanocomposites was observed proving by the presence of iron and zinc in the solution. But, at pH higher than pH_{pzc} (~7), the surface of nanocomposites will be negatively charged and As(III) exists mainly in form of $H_2AsO_3^-$, $HAsO_3^{2-}$ and AsO_3^{3-} anions (Sherlala A. I. A et al 2019; Su H et al 2017). For this reason, the sharp decrease in the arsenic adsorption capacity at pH range of 11-14 can be attributed to the electrostatic repulsion between the negative charged surface of the nanocomposites and the deprotonated anionic arsenic. However, this issue is having many different discussions (Sherlala A. I. A et al 2019; Su H et al 2017; Jiahua Zhu et al 2012; Blain Paul et al 2014; Fei Yu et al 2014). But above experimental results show it's suggested the de-adsorption process of S_0, S_1, S_2 and S_3 should be conducted in solution at pH 14 to reused.

As above analyzed results, the best arsenic adsorption occurs in a neutral environment (pH 7), where the inelastic exchange interaction takes place, which has the source of the Van der Waal interaction between the magnetic nanoparticles and adsorbent. Thus, maximum arsenic adsorption capacity was investigated by the Langmuir isotherm mode at 300 K in environment with pH 7

Maximum arsenic adsorption capacity

Equilibrium time of As(III) adsorption was analyzed by measurements of remaining arsenic concentrations in solution pH 7 after each different stirring intervals in inset of Fig. 7 (after 10, 15, 20, 25, 35 and 50 minutes). By the Langmuir isotherm equation at pH 7, the observation of maximum arsenic adsorption capacity using S_0, S_1, S_2 and S_3 samples at 300 K were performed. Unit of measurement of remained arsenic content C_f (in Fig. 7) is 1 ppb and in inset of Fig. 7 is 1 mg/L (Note: 0.001 mg/L = 1 ppb and the allowed arsenic level of 10 ppb regulated by the World Health Organization -WHO, European Commission - EC and United States Environmental Protection Agency - US EPA).

The observed results show that the minimum time to reach adsorption equilibrium is 20 minutes in pH 7 solution. Due to the porosity of S_0 sample and PANI coating in nanocomposite samples and inelastic collision in adsorption process, so the minimum adsorption equilibrium time is small compared with other iron sludge samples (Huiping Zeng et al 2020)

As shown in *Fig. 8*, the minimum arsenic contents remained in the equilibrium state with the minimum adsorption time is 20 minutes at room temperature. Thus the q_{max} (mg/g) maximum adsorbed arsenic amount per unit mass of adsorbent at equilibrium time is calculated by the Langmuir isotherm equation at pH 7 and 300 K (Khodabakhshi A et al 2011; Ruijiang Liu et al 2013; Babu CM et al 2013) with the first order linear relation:

$$\frac{C_f}{q} = \frac{1}{q_{max}} C_f + \frac{1}{b.q_{max}} \qquad (4)$$

where C_f: the remaining arsenic content (mg/L) at equilibrium state; q (mg/g) is the adsorbed arsenic amount per unit mass of adsorbent (S_0, S_1, S_2 and S_3) at the time of equilibrium; b ($L.mg^{-1}$): constants attributed to the interaction of adsorbed arsenic and adsorb compounds. The calculated values of q_{max} for S_0, S_1, S_2 and S_3 are presented in Table 4.

As in Table 4, the maximum arsenic adsorption capability q_{max} of S_1 was better than that of S_0 ($Fe_{0.90}Zn_{0.10}Fe_2O_4$) sample and Fe_3O_4 that reported in some works (Khodabakhshi A et al 2011; Minh Thi Tran et al 2016) with the same condition. In addition, the q_{max} value of S_1 is equivalent to the result in recent work (using chitosan magnetic graphene oxide nanocomposite) (Sherlala A. I. A et al 2019) and is larger than q_{max} values in other works (using core–shell Fe_3O_4@SiO_2 nanoparticles or magnetic graphene nanoplatelet with core-shell Fe@Fe_2O_3 nanoparticles) (Babu CM et al 2013; Jiahua Zhu et al 2012). The research results show that the combinations of co-precipitation method and in-situ polymerization method are very suitable to fabricate PANI/$Fe_{0.90}Zn_{0.10}Fe_2O_4$ magnetic nanocomposite materials to meet wastewater treatment and other technical applications (battery electrode, electromagnetic wave absorbing material).

Conclusion

The PANI/$Fe_{0.90}Zn_{0.10}Fe_2O_4$ nanocomposite materials were successfully synthesized by simple process with different mass ratios. These nanocomposite materials with large saturated magnetic moments and high specific surface area that contribute to its effective arsenic (III) adsorbing capability in aqueous solutions. The pH 7 level and minimum adsorption equilibrium time of 20 minutes are suitable factors for a best adsorption process. The sample S_1 with arsenic adsorption capacity (q_{max} = 43.48 mg/g) is highest than that of S_0, S_2, S_3 samples and many other magnetic nanomaterial types. In addition, due to the improving of saturation magnetization and chemical stability of nanomaterials, this work suggests the ability for heavy metal ion adsorption at pH 7 media and the desorption in strong alkaline solution of pH 14, then the materials could reabsorb for further trials.

Declarations

ACKNOWLEDGMENT

Funding: This work was supported by Nafosted project code 103.02-2021.37.

Author contributions:

Synthesization of samples, TGA measurements of samples: Vu Quoc Manh, Duong Khanh Linh

XRD and magnetization measurements: Do Khanh Tung, Nguyen Thuy Chinh and Thai Hoang

Investigation of absorption, software: Nguyen Manh Nghia, Duong Quoc Van,

Measurements of FT-IR, draft writing: Nguyen Thi Bich Viet,

The methodology, designed writing: Tran Minh Thi, editing: Vu Quoc Trung

Ethical approval: The authors confirm that the manuscript has been read and approved by all authors.

Consent to participate: All authors agreed to participate and reading the paper.

The authors declare that this manuscript has not been published and not under consideration for publication elsewhere.

Compliance with ethical standards

Conflict of interest: The authors declare that they have no conflict of interest in this manuscript.

References

1. Amir Aziz (2020) Green Synthesis of Fe_3O_4 Nanoparticles and Its Application in Preparation of Fe_3O_4/Cellulose Magnetic Nanocomposite: A Suitable Proposal for Drug Delivery Systems. Journal of Inorganic and Organometallic Polymers and Materials. https://doi.org/10.1007/s10904-020-01500-1
2. Adeleke J. T, Theivasanthi T, Thiruppathi M, Swaminathan M, Akomolafe T, Alabi A. B (2018) Photocatalytic Degradation of Methylene Blue by ZnO/$NiFe_2O_4$ Nanoparticles. *Applied Surface Science* 2018, https://doi.org/10.1016/j.apsusc.2018.05.184
3. Aparna M. L, Grace A. N, Sathyanarayanan P, Sahu N. K (2018) A comparative study on the supercapacitive behaviour of solvothermally prepared metal ferrite (MFe_2O_4, M=Fe, Co, Ni, Mn, Cu, Zn) nanoassemblies, *Journal of Alloys and Compounds* 2018, https://doi:10.1016/j.jallcom.2018.02.127.
4. Babu CM, Palanisamy B, Sundaravel B, Palanichamy M, and Murugesan V (2013) A Novel Magnetic Fe_3O_4/SiO_2 Core–Shell Nanorods for the Removal of Arsenic. Journal of Nanoscience and Nanotechnology 13, 2013, 2517-2527. https:// DOI: 10.1166/jnn.2013.7376
5. Blain Paul, Vyom Parashar and Ajay Mishra (2014) Graphene in the Fe_3O_4 nano-composite switching the negative influence of humic acid coating into an enhancing effect in the removal of arsenic from

water. Environ. Sci. Water Res. Technol., 2014, https://doi:10.1039/c4ew00034j

6. Bogdan Butoi, Andreea Groza, Paul Dinca, Adriana Balan and Valentin Barna. (2017) Morphological and Structural Analysis of Polyaniline and Poly(*o*-anisidine) Layers Generated in a DC Glow Discharge Plasma by Using an Oblique Angle Electrode Deposition Configuration. Polymers 2017, 9, 732; https://doi:10.3390/polym9120732
7. Chao Lian, Zhuo Wang, Rui Lin, Dingsheng Wang, Chen Chen, and Yadong Li (2017) An efficientfficient, controllable and facile two-step synthesis strategy: Fe_3O_4@RGO composites with various Fe_3O_4 nanoparticles and their supercapacitance properties. *Nano Research https://*doi.10.1007/s12274-017-1543-8
8. Cîrcu M, Radu T, Porav A. S, Turcu R (2018) Surface functionalization of Fe3O4@SiO2 coreshell nanoparticles with vinylimidazole-rare earth complexes: synthesis, physico-chemical properties and protein interaction effects, *Applied Surface Science* 2018, https://doi.org/10.1016/j.apsusc.2018.05.096
9. Deepshikha Rathore, Rajnish Kurchania, Pandey RK (2013) Structural, Magnetic and Dielectric Properties of $Ni_{1-x}Zn_xFe_2O_4$ (x=0, 0.5 and 1) Nanoparticles Synthesized by Chemical Co-Precipitation Method, Journal of Nanoscience and Nanotechnology 13, 2013, 812-1819. https:// doi:10.1166/jnn.2013.7120
10. Fizesan I, Iacovita C. Pop A. Kiss B. Dudric R. Stiufiuc R. Lucaciu C.M. Loghin F (2021) The Effect of Zn-Substitution on the Morphological, Magnetic, Cytotoxic, and In Vitro Hyperthermia Properties of Polyhedral Ferrite Magnetic Nanoparticles. *Pharmaceutics* **2021**, *13*, 2148. https://doi.org/10.3390/pharmaceutics13122148
11. Fei Yu, Sainan Sun, Jie Ma, Sheng Han (2014) Enhanced removal performance of arsenate and arsenite by magnetic graphene oxide with high iron oxide loading. Physical Chemistry Chemical Physics, 2014. https://DOI: 10.1039/C4CP04835K
12. Gabal M. A, Juaid A. A. Al, Rashed S. El, Hussein M. A, Angari Y. M. Al (2018) Polyaniline/$Co_{0.6}Zn_{0.4}Fe_2O_4$ core-shell nano-composites. Synthesis, characterization and properties. Journal of Alloys and Compounds 747, 2018, 83e90. https://doi.org/10.1016/j.jallcom.2018.02.316
13. Genç F, Turhan E, Kavas H, Topal U, Baykal A, Sözeri H (2015) Magnetic and Microwave Absorption Properties of $Ni_xZn_{0.9-x}Mn_{0.1}Fe_2O_4$ Prepared by Boron Addition, Journal of Superconductivity and Novel Magnetism 28, 2015, 1047-1050. https://DOI 10.1007/s10948-014-2670-5
14. Huda Faker, Yi-Fong Pan, Tsair-Fuh Lin (2015) Effect of Humic Acid on Arsenic Adsorption and Pore. Blockage on Iron-Based Adsorbent, Water Air Soil Pollut. 226, 2015, 14. https://DOI 10.1007/s11270-014-2224-2
15. Huiping Zeng, Longxue Zhai, Tongda Qiao, YapingYu, Jie Zhang & Dong Li (2020) Efficient removal of As(V) from aqueous media by magnetic nanoparticles prepared with Iron-containing water treatment residuals. Scientific Reports**.** https://doi.org/10.1038/s41598-020-65840-1
16. Jun Liu, Yuezhen Bin, and Masaru Matsuo (2012) Magnetic behavior of Zn-doped Fe_3O_4 nanoparticles estimated in terms of crystal domain size, Journal of Physical Chemistry C116

2012,134-143. https://doi.org/10.1021/jp207354s

17. Jiahua Zhu, Rakesh Sadu, Suying Wei, Daniel H. Chen, Neel Haldolaarachchige, Zhiping Luo, J. A. Gomes, David P. Young, and Zhanhu Guo (2012) Magnetic Graphene Nanoplatelet Composites toward Arsenic Removal. ECS Journal of Solid State Science and Technology, **1** (1) M1-M5, 2012, https://doi:10.1149/2.010201jss
18. Khodabakhshi A, Amin MM, Mozaffari M (2011) Synthesis of magnetic nanoparticles and evaluation of its efficiency for arsenic removal from simulated industrial wastewater, Iran J. Environ. Health. Sci. Eng 8, 2011, 189-200.
19. Kuen-Song Lin, Khalilalrahman Dehvari, Yeu-Jye Liu, Hua Kuo, and Pei-Ju Hsu (2013) Synthesis and Characterization of Porous Zero-Valent Iron Nanoparticles for Remediation of Chromium-Contaminated Wastewater, Journal of Nanoscience and Nanotechnology 13, 2013, 2675-2681. https://DOI: https://doi.org/10.1166/jnn.2013.7381
20. Kiril D. Hristovski, Jasmina Markovski (2017) Engineering metal hydroxide sorbents for removal of arsenate and similar weak-acid oxyanion contaminants: A critical review with emphasis on factors governing sorption processes. Science of The Total Environment, Vol. 598, 15 Nov. 2017, p. 258–271. https://DOI: 10.1016/j.scitotenv.2017.04.108
21. Lixin Yu, Xiaolin Lan, Changhong Wei, Xiang Li, Xiaoyan Qi, Tianyuan Xu, Chengjun Li, Chao Li, Zhijiang Wang (2018) MWCNT/NiO-Fe_3O_4 hybrid nanotubes for efficient electromagnetic wave absorption. Journal of Alloys and Compounds 748 (2018) 111e116. https://doi.org/10.1016/j.jallcom.2018.03.147
22. Lei Chen, Hongchuan Xin, Yuan Fang, Cong Zhang, Feng Zhang, Xing Cao, Chunhui Zhang, and Xuebing Li (2014) Application of Metal Oxide Heterostructures in Arsenic Removal from Contaminated Water. Journal of Nanomaterials Vol. 2014, Article ID 793610, 10 pages. https://doi.org/10.1155/2014/793610
23. Lia Méndez-Rodríguez, Tania Zenteno-Savín, Baudilio Acosta-Vargas, Jobst Wurl, Miguel Imaz-Lamadrid (2013) Differences in arsenic, molybdenum, barium, and other physicochemical relationships in groundwater between sites with and without mining activities, Natural Science 5, 2013, 238-243. https://DOI: 10.4236/ns.2013.52A035
24. Larumbe S., Gómez-Polo C., Pérez-Landazábal JI, García-Prieto A, Alonso J., Fdez-Gubieda M.L., Cordero D, and Gómez J (2012) Ni Doped Fe_3O_4 Magnetic Nanoparticles, Journal of Nanoscience and Nanotechnology 12, 2012, 2652-2660. https:// DOI: 10.1166/jnn.2012.5769
25. Mohamed Alae Ait Kerroum, Cristian Iacovita, Walid Baaziz, Dris Ihiawakrim, Guillaume Rogez, et al. (2021) Quantitative Analysis of the Specific Absorption Rate Dependence on the Magnetic Field Strength in $Zn_xFe_{3-x}O_4$ Nanoparticles. International Journal of Molecular Sciences, MDPI, 2020, 21(20), pp.7775. https://hal.archives-ouvertes.fr/hal-03365361
26. Minh Thi Tran, Thi Huyen Trang Nguyen, Quoc Trung Vu, and Minh Vuong Nguyen, (2016) Properties of poly(1-naphthylamine)/Fe_3O_4 composites and arsenic adsorption capability in wastewater. Front. Mater. Sci. 10, 2016, 56-65. https://doi.org/10.1007/s11706-016-0320-5

27. Park J. W, Jang A. N, Song J. H, Park C. Y, and Lee Y. S (2013) Electronic Structure of Zn Doped Fe_3O_4 Thin Films. Journal of Nanoscience and Nanotechnology 13. 2013, 1895-1898. https://doi.org/10.1166/jnn.2013.6996
28. Paul A. Webb, Clyde Orr, contributors: Ronnie W. Camp, James P. Olivier, Y. Simon Yunes, (1997) Analytical methods in fine particle technology, Micromeritics Instrument Corporation, Norcross, GA USA (1997), 60-62.
29. Ruijiang Liu, Yi Lu, Xiangqian Shen, Xinchun Yang, Xuewen Cui, and Yingying Gao (2013) Adsorption Kinetics and Isotherms of Arsenic(V) from Aqueous Solution On to $Ni_{0.5}Zn_{0.5}Fe_2O_4$ Nanoparticles, Journal of Nanoscience and Nanotechnology 13, 2013, 2835-2841. https:// DOI: 10.1166/jnn.2013.7392
30. Shah M. T, Alveroglu E, Balouch A, (2018) Pyranine functionalized Fe_3O_4 nanoparticles for the sensitive fluorescence detection of Cu^{2+} ions, *Journal of Alloys and Compounds* 2018, https://doi: 10.1016/j.jallcom.2018.06.334.
31. Sudheesh V. D, Thomas N, Roona N, Choudhary H, Sahoo B, Lakshmi N, Sebastian V (2018) Synthesis of nanocrystalline spinel ferrite (MFe_2O_4, M = Zn and Mg) by solution combustion method: Influence of fuel to oxidizer ratio, *Journal of Alloys and Compounds* 2018, htts://doi:10.1016/j.jallcom.2018.01.266
32. Sadia Ameen, M. Shaheer Akhtar, Young Soon Kim, O-Bong Yang, Hyung-Shik Shin (2010) Synthesis and characterization of novel poly(1-naphthylamine)/zinc oxide nanocomposites: Application in catalytic degradation of methylene blue dye, Colloid Polym. Sci. 288, 2010, 633-1638. https://DOI:10.1007/S00396-010-2284-9
33. Sherlala A. I. A, Raman, A. A. A., Bello M. M., Buthiyappan A (2019) Adsorption of arsenic using chitosan magnetic graphene oxide nanocomposite. Journal of Environmental Management, 246 (2019), 547–556. https://DOI: 10.1016/j.jenvman.2019.05.117
34. Su, H., Ye, Z., Hmidi, N. (2017) High-performance iron oxide-graphene oxide nanocomposite adsorbents for arsenic removal. Colloids Surfaces A Physicochem. Eng. Asp. 522, 2017, 161–172. https://DOI. 10.1016/j.colsurfa.2017.02.065
35. Tran Minh Thi., Nguyen Thi Huyen Trang, Nguyen Thi Van Anh (2015) Effects of Mn, Cu doping concentration to the properties of magnetic nanoparticles and arsenic adsorption capability in wastewater, Applied Surface Science 340, 2015,166-172. https://doi.org/10.1016/j.apsusc.2015.02.132
36. Tran Minh Thi, Vu Quoc Trung, D. K. Tung, et al (2021) Effect of Zn nonmagnetic element doping and a polyvinyl pyrrolidone shell layer on the superparamagnetism and stability properties of magnetic nanoparticles. Japanese Journal of Applied Physics 60, 025001, 2021, https://doi.org/10.35848/1347-4065/abd86d
37. Uwamariya V, Petrusevski B, Slokar YM, Aubry C, Lens PNL and Amy GL (2015) Effect of Fulvic Acid on Adsorptive Removal of Cr(VI) and As(V) from Groundwater by Iron Oxide-Based Adsorbents. Water Air Soil Pollut. 226, 2015, 184. https:// **DOI.**10.1007/s11270-014-2193-5

38. Xiaolong Li, Fengqin Zhang, Chao Ma, Elingarami Saul, and Nongyue He (2012) Green Synthesis of Uniform Magnetite (Fe_3O_4) Nanoparticles and Micron Cubes, Journal of Nanoscience and Nanotechnology 12, 2012, 2939-2942. https://doi.org/10.1166/jnn.2012.5684
39. Zapotoczny B., Dudek M.R., Guskos N, Kozioł JJ, Padlyak BV, Ko´smider M, and Rysiakiewicz-Pasek E (2012) FMR Study of the Porous Silicate Glasses with Fe_3O_4 Magnetic Nanoparticles Fillers. Journal of Nanomaterials Vol. 2012, Article ID 341073, 1-7. https://doi.org/10.1155/2012/341073
40. Zaki H. M, Heniti, Ahmad Umar, Marzouki F. Al, Abdel-Daiem A, Elmosalami T. A, Dawoud H. A, Hazmi F. S. Al, and Ata-Allah S. S (2013) Magnesium-Zinc Ferrite Nanoparticles: Effect of Copper Doping on the Structural, Electrical and Magnetic Properties, Journal of Nanoscience and Nanotechnology 13, 2013, 4056-4065. https:// DOI: 10.1166/jnn.2013.7434

Figures

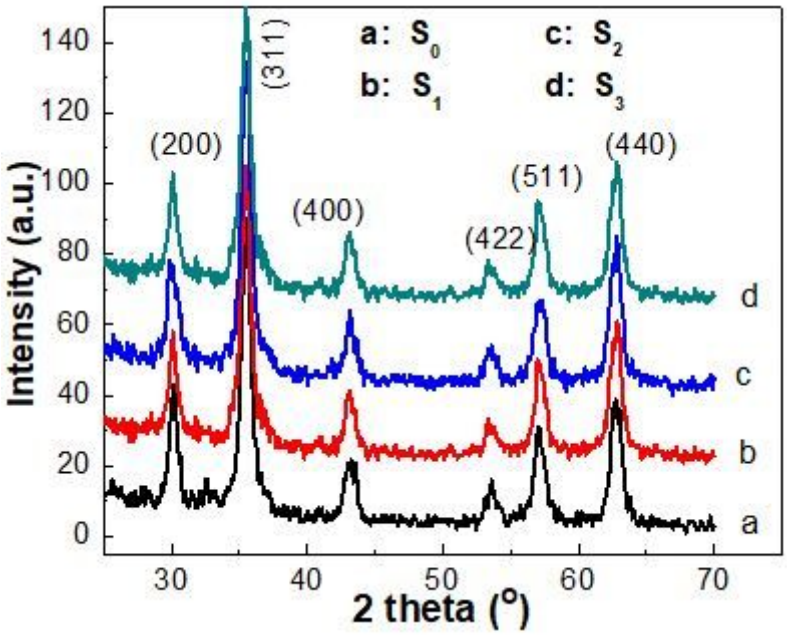

Figure 1

XRD patterns of S_0, S_1, S_2 and S_3

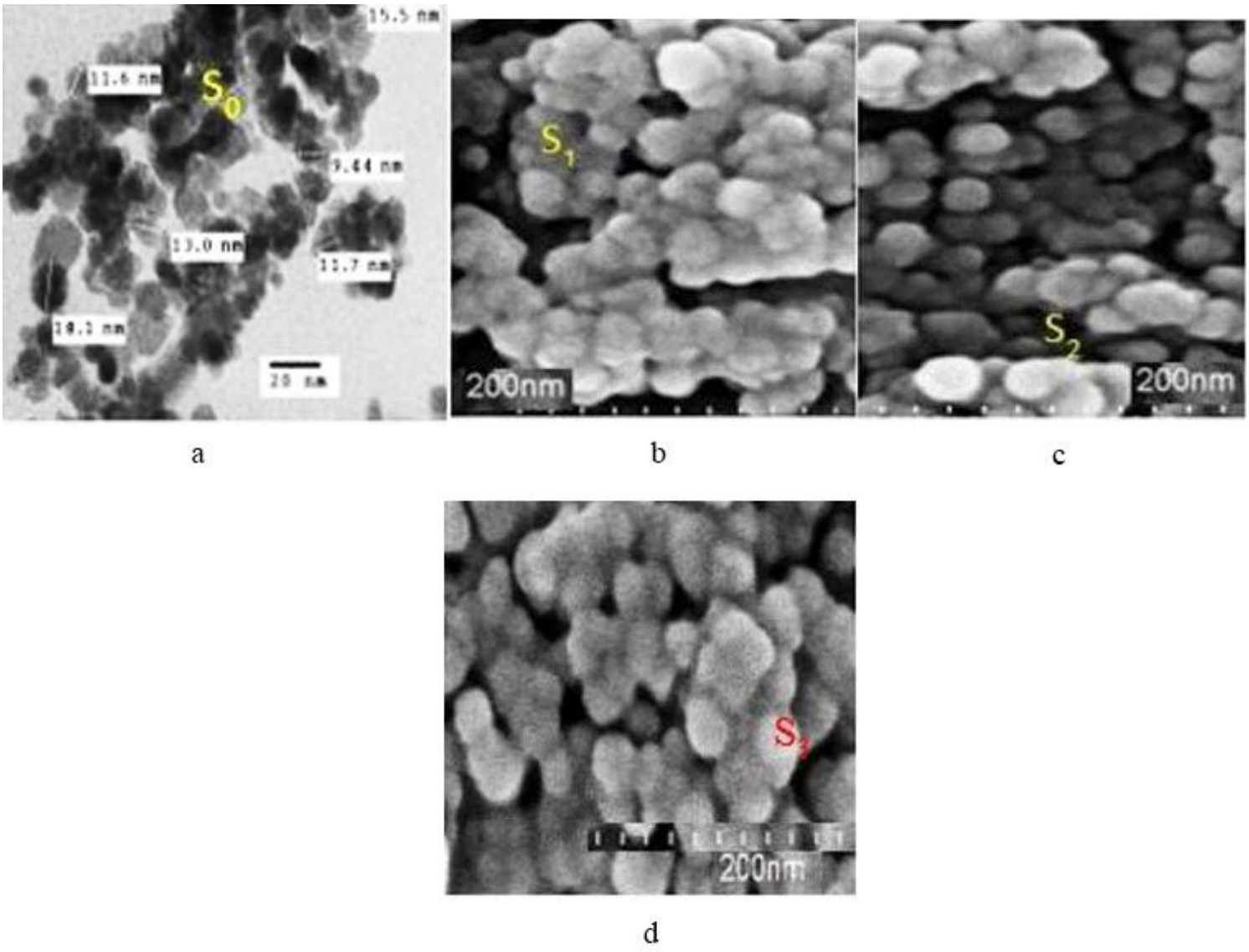

Figure 2

TEM image of S_0 (a), SEM images of S_1 (b), S_2 (c) and S_3 (d)

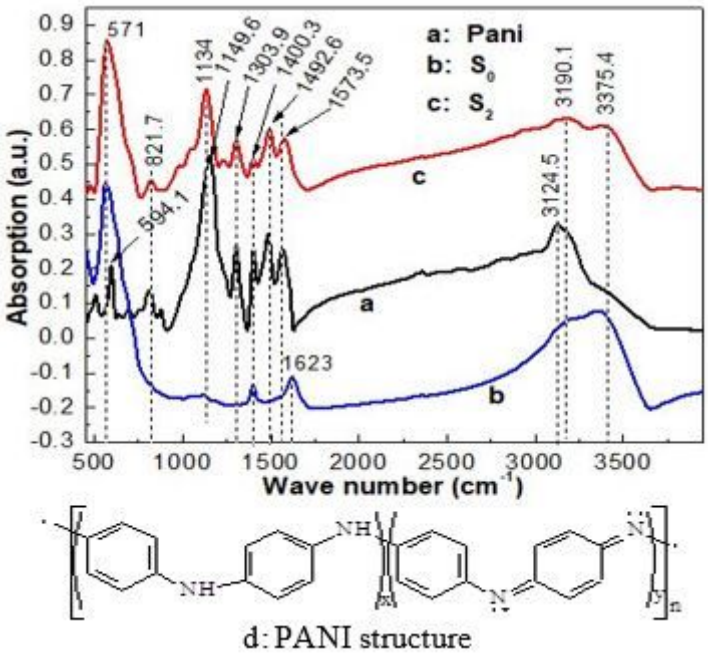

d: PANI structure

Figure 3

FT-IR spectra of samples: a, PANI, b: S_0, c: S_2 and d: PANI structure

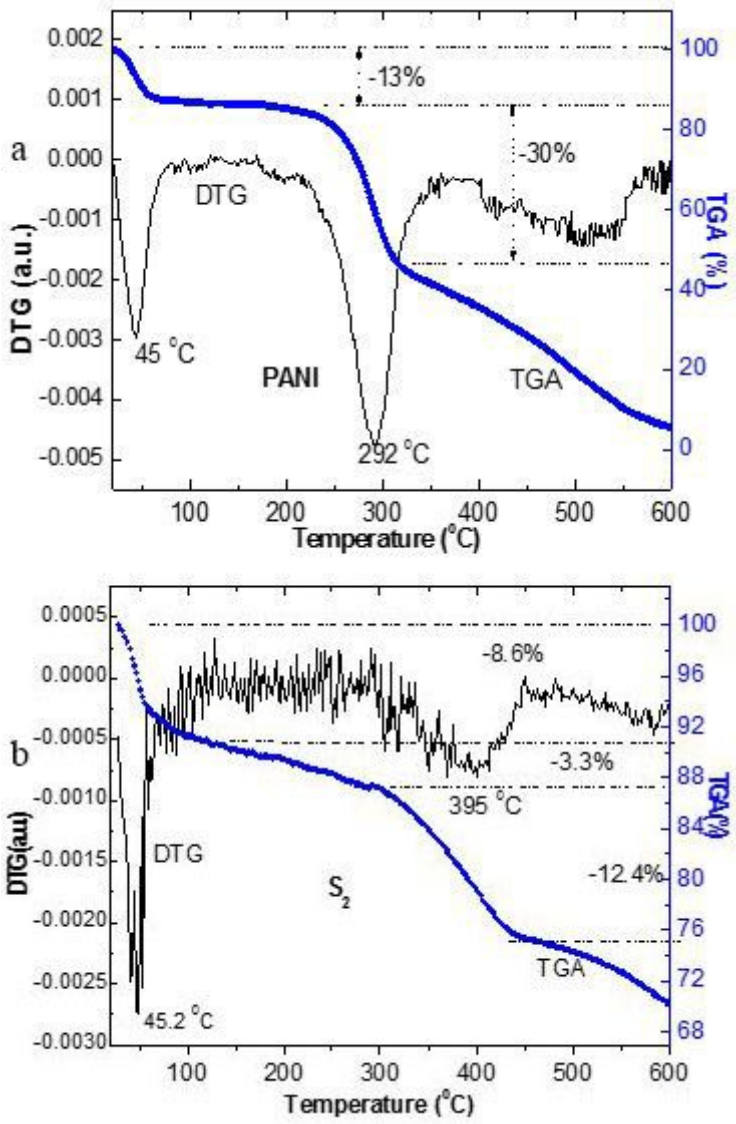

Figure 4

TGA and DTG Analyses of samples: a). PANI, b). S_2

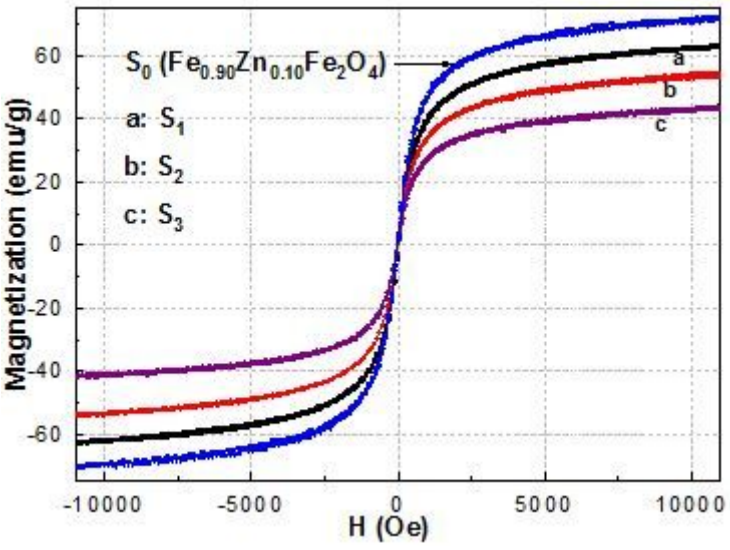

Figure 5

Magnetization curves of S_0, S_1, S_2 and S_3

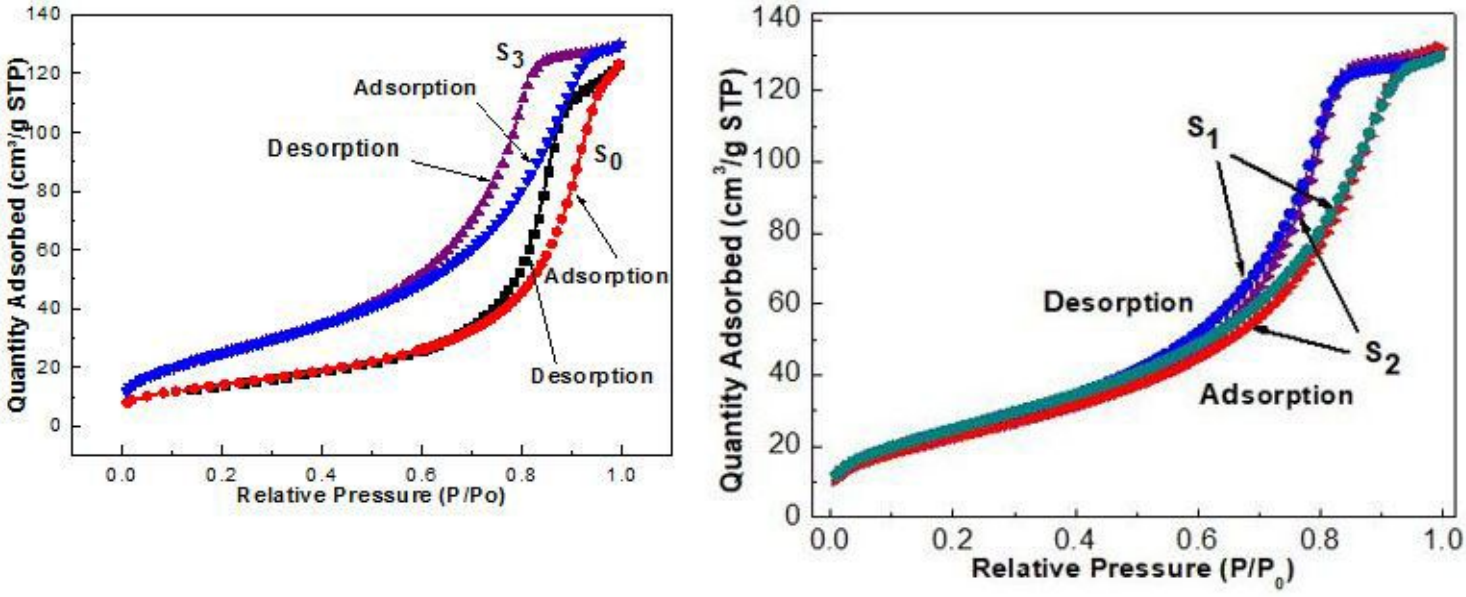

Figure 6

N_2 adsorption–desorption isotherm curves of samples

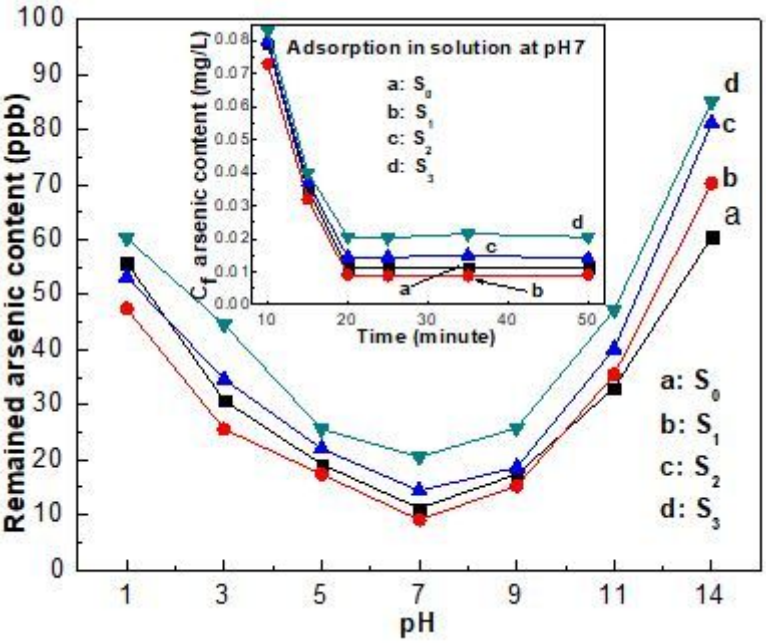

Figure 7

Remaining arsenic content as a function of pH. Inset: Remained arsenic content C_f in solution at pH 7

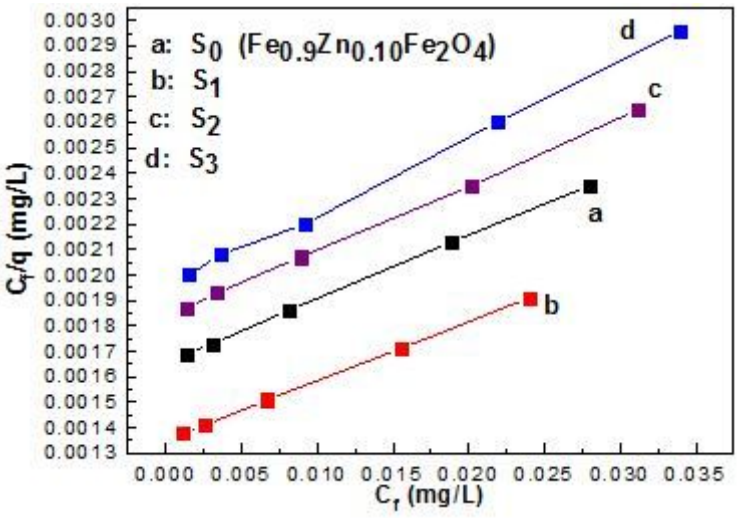

Figure 8

The C_f/q dependence on C_f using S_0, S_1, S_2 and S_3 with different PANI/$Fe_{0.9}Zn_{0.1}Fe_2O_4$ mass ratios